Theory of Size-Dependent Resonance Raman Scattering from Carbon Nanotubes

Ernst Richter and K. R. Subbaswamy*

Department of Physics and Astronomy, University of Kentucky, Lexington, Kentucky 40506-0055

(Received 26 March 1997)

Raman scattering from single-walled carbon nanotubes is examined in detail theoretically and compared with experiments. Within a simple tight-binding model the Raman matrix elements are evaluated explicitly, and the shape of the resonance in the scattered intensity due to interband electronic transitions is derived. The resonance in the optical regime is shown to depend sharply on the diameter of the tubes. Thus, resonance Raman scattering may be used for determining size distribution in a sample, as well as for the determination of details of the band structure. [S0031-9007(97)04252-X]

PACS numbers: 78.30.Na, 61.48.+c, 71.15.Fv

With the recent progress in methods for synthesizing samples containing high concentrations of single-walled nanotubes (SWNT) of carbon [1] it has become possible to probe the properties of these quasi-one-dimensional crystals in some detail [2]. The major components of these samples appear to be the so-called "armchair" achiral tubes with diameters of $\sim$13 Å, especially those designated as (10,10) tubes in the standard notation (see Fig. 1) [3,4].

In particular, the measurement of the Raman spectra of SWNT as a function of exciting laser wavelength has revealed some peculiar results: not only is there evidence for a resonant process (i.e., variation in the relative intensities of the spectral features), but the frequencies of the observed vibrational modes themselves appear to shift. The results were interpreted as evidence for the presence of a distribution of SWNT of different diameters, whose vibrational modes were selectively excited due to an electronic interband resonance which itself is diameter dependent [2]. This analysis was based solely on computed electronic density of states with no attention to the relevant Raman matrix elements. In this Letter we compute the matrix elements for the Raman process [5] for SWNT within a simple tight-binding model which is known to give an accurate description of the π-band structure of graphite. We confirm the qualitative aspects of the interpretation of recent experiments and make detailed predictions for the resonance shape, which should help in determining the tube composition of the samples by comparison with future experiments. Additionally, by measuring resonance shapes conclusions could be drawn on the actual electronic band structure and the behavior of the electron-phonon matrix elements. (Even though experimental Raman spectra obtained at various laser frequencies exist in the literature their absolute intensities are not related. Therefore, existing spectra cannot be used to construct resonance curves.)

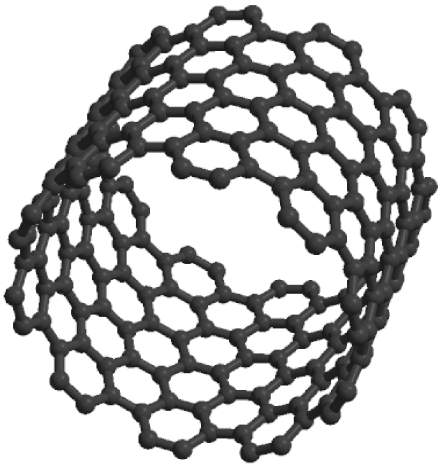

FIG. 1. Single-walled carbon nanotube with the (10,10) geometry in the standard notation (see Ref. [3]). Five unit cells are shown.

For our calculation we use the simple, zone-folding tight-binding model introduced in this context by Dresselhaus *et al.* [3,6]:

$$E(k_t, k) = \pm\gamma_0\left\{1 + 4\cos\left(\frac{\sqrt{3}k_t a_0}{2}\right)\cos\left(\frac{ka_0}{2}\right) + 4\cos^2\left(\frac{ka_0}{2}\right)\right\}^{1/2}, \quad (1)$$

where γ_0 is the nearest-neighbor carbon-carbon (C-C) overlap integral, and $a_0 = 1.42 \times \sqrt{3}$ Å is the lattice constant of the 2D graphene sheet. k is the wave vector of the one-dimensional lattice. We take $\gamma_0 = -2.5$ eV which is suggested by comparison with first-principles calculations [7]. The construction of the tube involves the restriction of the tangential wave vectors k_t corresponding to the two-dimensional lattice of the graphene sheet to a small number of discrete, quantized values, dependent on the diameter. Thus, for instance, for the (N,N) armchair tubes, the tangential wave vector values (k_t) are restricted to $\pi q/(N\sqrt{3}a_0)$, with $q = -N, \ldots, N-1$. From this restriction, one obtains the one-dimensional electronic bands. The band structure obtained in this manner for the (10,10) case is shown in Fig. 2(a). The corresponding density of states (DOS), Fig. 2(b) displays the singularities induced by the one-dimensional character of the bands. Using zone-folding arguments it can be shown [3] that all (N,N) tubes are semimetals (as displayed by the small, but nonzero DOS at the Fermi level).

 0031-9007/97/79(14)/2738(4)$10.00

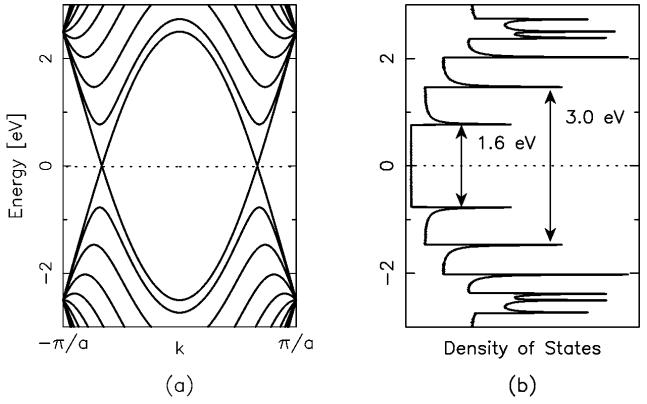

FIG. 2. (a) π-band structure for the (10,10) tube; (b) the corresponding density of states. The first two prominent interband transitions are indicated.

For calculating Raman spectra, we also need the phonon modes of the system. For this purpose, we have used empirical (up to fourth nearest-neighbor) force-constant parameters derived by Jishi *et al.* [8] by fitting to the phonons of a graphene sheet. The parameters have been transferred without change from the plane to the cylindrical geometry. The number of symmetry allowed Raman active zone-center modes (A_{1g}, E_{1g}, and E_{2g} modes according to their representation), which is independent of the tube diameter, is 16 for even values and 15 for odd values of N [3].

The scattering cross section is proportional to the squared modulus of the suitably contracted Raman tensor whose contributions are of the form [5]

$$R_{\sigma}^{ij} = \sum_{\alpha,\beta,\gamma} \frac{p_{\gamma\beta}^{i} p_{\beta\alpha}^{j} \Xi_{\sigma,\alpha\gamma}}{(\omega_I - \omega - \omega_{\beta\gamma})(\omega_I - \omega_{\alpha\beta})}, \quad (2)$$

where $p_{\alpha\beta}^{i}$ refer to the electron momentum matrix elements; $\Xi_{\sigma,\alpha\beta}$ refer to electron-phonon matrix elements; ω_I, ω_S, and ω refer, respectively, to the incident photon, the scattered photon, and phonon frequency. $\omega_{\alpha\beta}$ are the frequencies of the possible electronic transitions with α, β, γ labeling initial and intermediate electronic states. For the different contributions to the Raman tensor ω_I, ω_S, and ω in the energy denominator are permuted allowing for the incident or scattered photon to be possibly in resonance with an electronic transition. We have computed all relevant contributions within the finite temperature Green's function method [9]. All spectra shown in this paper correspond to room temperature.

The electron-phonon matrix elements are related to the deformation potential, and are introduced by a displacement dependence of the nearest-neighbor C-C overlap integral:

$$\gamma_0(|\vec{R} + \vec{u}|) = \gamma_0(|\vec{R}|) + \Delta \frac{\vec{R}}{|\vec{R}|} \cdot \vec{u}, \quad (3)$$

with $\vec{R}$ being the equilibrium bond vector. If we confine to nearest-neighbor interaction only, the constant Δ enters the calculation only as an overall scaling factor for the Raman intensities and, therefore, can be left unspecified. Another parameter needed is the excited electron lifetime, which we take to be 0.1 eV. The simple form of the electron-phonon matrix element chosen here contains only the deformation potential component, namely the coupling resulting from a volume change. Given the simplifying assumptions in our electronic model, a more complicated form would be unjustified, and would introduce additional parameters into the calculation.

The computed Raman spectra for (10,10) tubules are shown in Fig. 3 for two different incident laser frequencies. The Raman tensor was averaged over all possible tube orientations to account for the probably random orientations of the tube bundles in the experimental samples. Furthermore, we averaged over the polarization of incident and scattered light to account for the unpolarized scattering geometry used in experiments to maximize the intensity of the Raman signal. A linewidth of 10 cm^{-1} was assumed for all modes in computing the spectra. Notice the shift in relative intensity from the low frequency modes to the high frequency modes in going from 1.5 to 1.65 eV. Analysis of the various contributions to the Raman tensor shows that the calculated spectra are dominated by double resonant scattering in this region of the incident laser light. Within our simple nearest-neighbor approach only A_{1g} symmetry modes contribute with sufficient intensity: the (macroscopic) breathing mode (165 cm^{-1}) and the graphiticlike optic mode (1585 cm^{-1}). Note that both modes can be associated with zone center vibrations of the graphene sheet.

We now briefly discuss symmetry related selection rules and their effect on the spectra. Let the tube axis be along $\hat{z}$. Then, A_{1g} and E_{2g} modes can contribute only to the polarized spectrum [e.g., (z,z) geometry], while

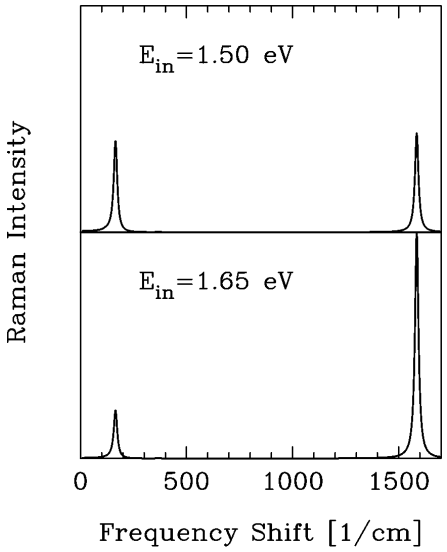

FIG. 3. Computed Raman spectra of (10,10) tubes at incident laser energy of 1.5 and 1.65 eV.

E_{1g} modes can contribute only to the depolarized spectrum [e.g., (z,x) geometry]. Since, as stated above, the calculated spectra are dominated by near double resonance scattering we focus on those contributions to the Raman tensor [Eq. (2)] that lead to the simultaneous near-vanishing of *both* factors in the denominator. Symmetry analysis and phase space considerations show that E_{1g} vibrational modes do not lead to a double resonance condition in any geometry. A_{1g} modes modulating vertical electronic transitions between the mth valence band maximum and the mth conduction band minimum can contribute in the (z,z) geometry while those modulating vertical electronic transitions between the mth maximum of the valence band and the $(m \pm 1)$th minimum of the conduction band can contribute in the (x,x) and (y,y) geometry, although at much lower intensity than in the former case. Similarly, E_{2g} modes can lead to near double resonance in the (z,z) geometry for valence-conduction band pairs of particular symmetry. In the (x,x) or (y,y) geometry these modes can lead to double resonance for electronic transitions to and from the Fermi level, but the low density of states at the Fermi level suppresses the Raman intensity.

In Fig. 4 the variation of the Raman peak intensities is shown as a function of the incident laser frequency for scattering from armchair tubes of three different diameters, namely, (8,8), (9,9), and (10,10). The solid line is for the low frequency breathing mode, and the dotted line is for the high frequency A_{1g} mode. Note that in each case the resonance effect is clearly displayed for both A_{1g} symmetry modes and points out the quasi-one-dimensional character of the tubules. As stated above, E_{1g} and E_{2g} modes do not contribute much intensity at this level of approximation. A comparison with Figs. 2(a) and 2(b) shows that the ith resonance [here in the case of (10,10) tubes] is due to electronic transitions between the ith maximum below and ith minimum above the Fermi level corresponding to singularities in the DOS. The positions of the intensity maxima for the low and high frequency A_{1g} modes are shifted due to their large frequency difference of $\sim 1400\ \mathrm{cm}^{-1}$ (0.17 eV). Small resonance peaks (which may not be clearly resolved on the scale of this figure) appear between the dominant peaks. They are related to the A_{1g} modulation of the electronic transitions between the mth maximum of the valence band and the $(m \pm 1)$th minimum of the conduction band, i.e., 1st $\longrightarrow$ 2nd or 2nd $\longrightarrow$ 1st; see the discussion of selection rules above.

Comparing the resonances for all three tubes we note that as the diameter of the tube increases the absolute intensities (shown for the first resonance) go down due to a lower DOS for this particular resonance transition. This behavior is expected due to the fact that in the limit of infinite diameter (graphene) the oscillator strength for this resonance should vanish. The resonance curves for tubes close in diameter overlap; therefore, vibrational modes corresponding to such tubes show up simultaneously in the spectra of a sample with a distribution of tube diameters. At laser frequencies of ~ 2.4 eV, the first resonance peak for the (8/8) tube slightly overlaps with the second one for the (10/10) tubes.

In Fig. 5 we show the simulated Raman spectra of an equal mixture of (8,8), (9,9), and (10,10) tubes at two different laser frequencies. In the upper portion ($E_{\mathrm{in}} = 1.55$ eV) of Fig. 5 the (10,10) tubes are close to a resonance, and their modes are much more prominent in the spectrum. In the lower portion ($E_{\mathrm{in}} = 1.90$ eV) the (8,8) tubes are close to resonance, and their modes are dominant in the spectrum. Therefore, in this particular interval for the energy of the incident laser the position of the breathing-mode peak shifts to higher frequency with increasing laser energy. For the chosen sample composition

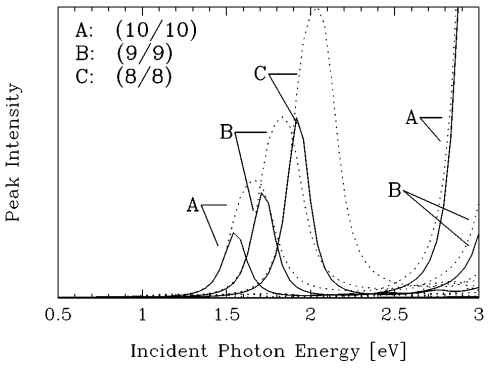

FIG. 4. Variation of the Raman peak intensities with photon energy; solid lines are for the low frequency breathing mode, and the dotted lines are for the high frequency graphitic A_{1g} mode.

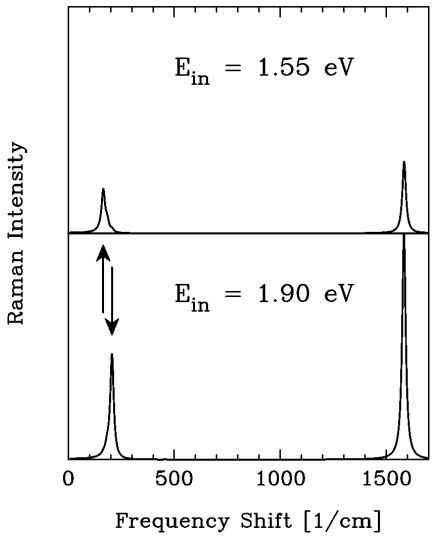

FIG. 5. Simulated Raman spectra for an equal mixture of (8,8), (9,9), and (10,10) tubes for incident laser energy of 1.55 and 1.9 eV. The arrows are drawn to draw attention to the apparent shift in the peak position.

and incident laser frequencies the peak corresponding to the breathing mode shifts by 41 cm^{-1}. This is a clear demonstration of the diameter-selective resonance effect that was invoked as a possible explanation of the Raman scattering from the purified SWNT samples observed by Rao *et al.* [2]. In these experiments shifts of the order of magnitude as shown in Fig. 5 have been observed for the position of the breathing mode peak. Note that the calculated frequency of the optical A_{1g} mode depends less strongly on the tube diameter than the frequency of the breathing mode. In going from the (8,8) to the (10,10) tubes, it is shifted upwards by roughly 7 cm^{-1}. The weaker dependence on the incident laser frequency of the position of the high frequency phonon peaks is in agreement with the experimental Raman spectra [2]. But the broader, overlapping peak structure in the observed spectra in the optical phonon region makes it harder to relate experimentally observed Raman peaks directly to specific vibrations in a certain type of nanotubes. For a unique analysis of the experimental spectra resonance curves over certain intervals of incident laser frequency will be necessary.

The simple expressions for the electronic band energies, Eq. (1), and for the deformation potential coupling, Eq. (3), do not fully account for all possible effects on the π band structure and electron phonon interaction in nanotubes, respectively. Curvature effects such as changes in the overlap due to orientational variations of neighboring p orbitals which are introduced by going from the flat graphene sheet to the cylindrical tube geometry are neglected in this nearest-neighbor model. Together with the actual value of the overlap, deviations of the electronic band structure from the idealized cosinelike behavior of Eq. (1) will alter the exact positions of the interband resonances. Even though curvature effects are present in our calculation of the vibrational modes the simplified treatment of the electrons may subject the Raman tensor to the more stringent selection rules of the graphene sheet. This latter fact may explain why in the present calculation A_{1g} modes, which can be related to zone center vibrations of the graphene sheet, dominate the Raman spectra. An analysis of the experimental spectra [2] suggests that, especially in the high frequency region, E_{2g} and E_{1g} modes which are related to folded (off zone center) graphene modes contribute to the spectra.

In conclusion, we have shown by explicit calculation within a simple, but realistic model, that the unique, one-dimensional nature of the single-walled carbon nanotubes gives rise to diameter-dependent electronic resonance effects that are clearly discernible in Raman scattering. The enhancement results from the (near) double resonance condition of the energy denominators of the Raman tensor for vertical transitions from the mth valence band maximum to the mth conduction band minimum. Even in an inhomogeneous sample, incident laser frequency may be tuned to select out the vibrational modes of specific tube types. Measurement of the resonance shape can be used to extract information on the electronic band structure [overlap parameter γ_0, deviations of the π band structure from Eq. (1)] and electron-phonon coupling in these systems. For instance, the energy separation between two successive resonances can be used to gauge the effect of σ-π hybridization due to the curvature of the graphene sheet. Since, according to the selection rules, Raman allowed modes of different symmetry differ in their resonance behavior resonance curves would also be useful for analyzing the broad, overlapping peak structure in the optical phonon frequency region.

In the present work we have focused only on Raman scattering off armchair (N,N) nanotubes. However, x-ray diffraction experiments suggest that a small amount of chiral nanotubes may also be present in the experimental sample [10]. For all nanotubes, the breathing mode is a macroscopic mode and its frequency is essentially determined by the diameter. The high frequency optical modes are determined by very local properties (i.e., the carbon bond stretch), with minor perturbation from the geometry. Thus, the primary difference due to the presence of chiral tubes should come from the intermediate frequency region, where these tubes might contribute to the spectrum with higher intensity due to less stringent selection rules. This might explain why experimental Raman spectra show a richer peak structure than obtained within our simple model description.

This research was supported in part by NSF Grant No. OSR 94-52895, and by the University of Kentucky Center for Computational Sciences. We thank Dr. Peter Eklund for valuable discussions.

*Present address: Department of Physics, University of Miami, Coral Gables, FL 33126.

[1] A. Thess *et al.*, Science **273**, 483 (1996).
[2] A. M. Rao *et al.*, Science **275**, 187 (1997).
[3] M. S. Dresselhaus, G. F. Dresselhaus, and P. C. Eklund, *Science of Fullerenes and Carbon Nanotubes* (Academic Press, New York, 1996).
[4] The numbers (n,m) refer to the integer multiples of the unit vectors of the two-dimensional graphite sheet needed to construct the spanning vector for the graphite strip from which the tube is derived by folding.
[5] W. Hayes and R. Loudon, *The Scattering of Light by Crystals* (John Wiley, New York, 1976).
[6] M. S. Dresselhaus, G. F. Dresselhaus, and R. Saito, Solid State Commun. **84**, 201 (1992).
[7] J. W. Mintmire and C. T. White, Carbon **33**, 893 (1995).
[8] R. A. Jishi, L. Venkataraman, M. S. Dresselhaus, and G. Dresselhaus, Phys. Rev. B **51**, 11 176 (1995).
[9] M. V. Klein, in *Light Scattering in Solids III*, edited by M. Cardona and G. Güntherodt (Springer, Berlin, 1982), p. 121.
[10] J. M. Cowley, P. Nikolaev, A. Thess, and R. E. Smalley, Chem. Phys. Lett. **265**, 379 (1997).